scientific reports

Check for updates

OPEN

Remodeling tumor microenvironment by liposomal codelivery of DMXAA and simvastatin inhibits malignant melanoma progression

Valentin-Florian Rauca[1,2], Laura Patras[1], Lavinia Luput[1], Emilia Licarete[1,3], Vlad-Alexandru Toma[1,4,5], Alina Porfire[6], Augustin Catalin Mot[7], Elena Rakosy-Tican[1], Alina Sesarman[1]✉ & Manuela Banciu[1]

Anti-angiogenic therapies for melanoma have not yet been translated into meaningful clinical benefit for patients, due to the development of drug-induced resistance in cancer cells, mainly caused by hypoxia-inducible factor 1α (HIF-1α) overexpression and enhanced oxidative stress mediated by tumor-associated macrophages (TAMs). Our previous study demonstrated synergistic antitumor actions of simvastatin (SIM) and 5,6-dimethylxanthenone-4-acetic acid (DMXAA) on an in vitro melanoma model via suppression of the aggressive phenotype of melanoma cells and inhibition of TAMs-mediated angiogenesis. Therefore, we took the advantage of long circulating liposomes (LCL) superior tumor targeting capacity to efficiently deliver SIM and DMXAA to B16.F10 melanoma in vivo, with the final aim of improving the outcome of the anti-angiogenic therapy. Thus, we assessed the effects of this novel combined tumor-targeted treatment on *s.c.* B16.F10 murine melanoma growth and on the production of critical markers involved in tumor development and progression. Our results showed that the combined liposomal therapy almost totally inhibited (> 90%) the growth of melanoma tumors, due to the enhancement of anti-angiogenic effects of LCL-DMXAA by LCL-SIM and simultaneous induction of a pro-apoptotic state of tumor cells in the tumor microenvironment (TME). These effects were accompanied by the partial re-education of TAMs towards an M1 phenotype and augmented by combined therapy-induced suppression of major invasion and metastasis promoters (HIF-1α, pAP-1 c-Jun, and MMPs). Thus, this novel therapy holds the potential to remodel the TME, by suppressing its most important malignant biological capabilities.

Abbreviations

ANOVA	Analysis of variance;
ARG-1	Arginase-1
AUTCs	Areas under the tumor growth curves

[1]Department of Molecular Biology and Biotechnology, and Center of Systems Biology, Biodiversity and Bioresources, Faculty of Biology and Geology, Babes-Bolyai University, 5-7 Clinicilor Street, 400006 Cluj-Napoca, Romania. [2]Department of Dermatology and Allergy, School of Medicine, Technical University of Munich, 29 Biedersteiner Street, 80802 Munich, Germany. [3]Molecular Biology Centre, Institute for Interdisciplinary Research in Bio-Nano-Sciences of Babes-Bolyai University, 42 Treboniu Laurian Street, 400271 Cluj-Napoca, Romania. [4]Department of Experimental Biology and Biochemistry, Institute of Biological Research, Branch of NIRDBS Bucharest, 48 Republicii Street, 400015 Cluj-Napoca, Romania. [5]Department of Molecular and Biomolecular Physics, National Institute of Research and Development for Isotopic and Molecular Technologies, 67-103 Donath Street, 400293 Cluj-Napoca, Romania. [6]Department of Pharmaceutical Technology and Biopharmaceutics, Faculty of Pharmacy, University of Medicine and Pharmacy "Iuliu Hatieganu", 8 Babeş Street, 400012 Cluj-Napoca, Romania. [7]Research Center for Advanced Chemical Analysis, Instrumentation and Chemometrics, Faculty of Chemistry and Chemical Engineering, Babes-Bolyai University, 11 Arany Janos Street, 400028 Cluj-Napoca, Romania. ✉email: sesarman@gmail.com

Bax	Bcl-2-associated X protein
Bcl-xL	B-cell lymphoma-extra-large
bFGF	Basic fibroblast growth factor
BRAF	V-Raf murine sarcoma viral oncogene homolog B1
CD31	Cluster of differentiation 31
CHL	Cholesterol
DMEM	Dulbecco's Modified Eagle's Medium
DMXAA	5,6-Dimethylxanthenone-4-acetic acid
DPPC	1,2-Dipalmitoyl-sn-glycero-3-phosphocholine
ECM	Extracellular matrix
PEG-2000-DSPE	(N-(Carbonyl-methoxypolyethylene-glycol-2000)-1,2-distearoyl-sn-glycero-3 phosphoethanolamine, sodium salt)
EPR	Enhanced permeability and retention
FasL	Fas ligand
G-CSF	Granulocyte-colony stimulating factor
GM-CSF	Granulocyte-macrophage-colony stimulating factor
HE	Hematoxylin and Eosin
HIF-1α	Hypoxia-inducible factor 1α
HPLC	High-Performance Liquid Chromatography
HRP	Horseradish peroxidase
iNOS	Inducible nitric oxide synthase
IFN-γ	Interferon γ
IGF-II	Insulin-like growth factor 2
IL-12p40	Interleukin 12 p40
IL-12p70	Interleukin 12 p70
IL-13	Interleukin 13
IL-1α	Interleukin 1α
IL-1β	Interleukin 1β
IL-6	Interleukin 6
IL-9	Interleukin 9
i.v.	Intravenous
LCL	Long circulating liposomes
MCP-1	Monocyte chemoattractant protein-1
M-CSF	Monocyte-colony stimulating factor
MDA	Malondialdehyde
MIG	Monokine induced by IFN-γ
MMPs	Matrix metalloproteinases
MMP-2	Matrix metalloprotease-2
MMP-9	Matrix metalloprotease-9
pAP-1 c-Jun	Phosphorylated form of c-Jun subunit of AP-1
PBS	Phosphate buffered saline
PF-4	Platelet factor 4
MEK	Mitogen-activated protein kinase kinase
PDI	Polydispersity index
ROS	Reactive oxygen species
s.c.	Subcutaneous
SD	Standard deviation
SDS	Sodium dodecyl sulfate
SIM	Simvastatin
TAC	Total antioxidant capacity
TAMs	Tumor-associated macrophages
TBS-T	Tris Buffered Saline with Tween
TIMP-1	Tissue inhibitor of metalloproteinase 1
TIMP-2	Tissue inhibitor of metalloproteinase 2
TME	Tumor microenvironment
TNF-α	Tumor necrosis factor α
VDA	Vascular disrupting agent
VEGF	Vascular endothelial growth factor

Melanoma cells are established providers of essential growth factors to trigger tumor angiogenesis, such as VEGF and bFGF that further support tumor development and metastasis[1,2]. Therefore, targeting tumor vasculature with anti-angiogenic drugs such as vascular disrupting agents (VDA) seemed like a promising approach in the treatment of solid tumors, albeit drug resistance associated with anti-angiogenic therapy was reported in most of the cases[3,4]. Especially after VDA treatment, a remaining viable tumor rim, characterized by intratumor overexpression of hypoxia-inducible factor 1α (HIF-1α) and enhanced oxidative stress mediated by tumor-associated macrophages (TAMs), is responsible for selecting aggressive tumor cell phenotypes ready to escape oxygen and nutrient deprivation and thus, accelerating the undesired outcome of the disease[4–6]. Moreover, our previous findings have shown that simvastatin (SIM)-a lipophilic statin incorporated in long-circulating

liposomes (LCL-SIM) could counteract both causes of cancer resistance to anti-angiogenic treatments as LCL-SIM inhibited B16.F10 murine melanoma growth in vivo via suppression of TAMs-mediated oxidative stress and HIF-1α levels in melanoma cells[7]. Thus, the involvement of intratumor macrophages in tumor cell resistance to apoptosis and chemotherapy might be exploited for future TAMs-targeted therapies that can counteract negative outcomes of the anti-angiogenic treatments[8]. Furthermore, in another recent study, when we administered SIM in combination with a VDA, 5,6-dimethylxanthenone-4-acetic acid (DMXAA), the aggressiveness of melanoma cells was suppressed due to the synergistic action on cancer cell proliferation as well as inhibition of protumor function of TAMs in vitro[9]. In tight connection with these data, it has been shown recently that the combination between an anti-angiogenic agent and an antioxidant modulator could counteract the effect of HIF on cancer cell metabolism[10]. Targeting the mediators of communication between cancer cell and cells residing the TME may successfully complement other treatment alternatives[11].

In the present study, we aimed to improve the outcome of anti-angiogenic therapy for B16.F10 melanoma in vivo by using a novel tumor-targeted approach based on codelivery of liposomal DMXAA together with liposomal SIM. To our knowledge, this therapeutic approach has never been described before. We evaluated the effects of this combined tumor-targeted treatment on *s.c.* B16.F10 murine melanoma growth, with regard to the levels of specific markers involved in angiogenesis, inflammation, oxidative stress, apoptosis, invasion and metastasis. Our results showed that this novel targeted therapy holds the potential to remodel the TME, by suppressing its most important malignant biological capabilities.

Materials and methods

Preparation and physicochemical characterization of liposomal formulations. DPPC and PEG-2000-DSPE were acquired from Lipoid GmbH (Ludwigshafen, GER), CHL and SIM from Sigma-Aldrich Chemie GmbH (Munich, GER) and DMXAA was purchased from Selleck Chemicals LLC (Houston, TX). The molar ratio of compounds used for LCL-SIM preparation was 17:1.01:1:1.209 (DPPC:PEG-2000-DSPE:CHL:SIM), according to our previous published protocols[7]. The molar ratio of compounds used for the preparation of the novel DMXAA liposomal formulation was 1.85:0.7:0.3:0.15 (DPPC:CHL:DMXAA:PEG-2000-DSPE) and was based on previous studies regarding nanoformulations that encapsulated small molecule therapeutic agents[12,13]. Lipid film hydration method followed by multiple extrusion steps was used to prepare nanoliposomes as described previously[7]. Each LCL formulation was characterized as size, polydispersity index, zeta potential, the concentration of the active drug, and entrapment efficiencies.

Cell type and murine tumor model. B16.F10 murine melanoma cells (ATCC, CRL-6475) were cultured in DMEM according to our previously described methods[9]. Syngeneic male C57BL/6 mice 6 to 8-week-old (Cantacuzino Institute, Bucharest, RO) kept under standard laboratory conditions were inoculated with 1×10^6 B16.F10 cells *s.c.* in the right flank. Tumor size and body weight were monitored on a daily basis during treatment. Tumor volume was assessed using the formula $V = 0.52a^2b$, where a is the smallest and b is the largest superficial diameter of the tumor[14]. Treatments started at day 11 after cell inoculation when tumors were about 140 mm^3. To measure the antitumor efficiency of the combined liposomal administration of 5 mg/kg SIM and 14 mg/kg DMXAA in comparison with liposomal monotherapy of either 5 mg/kg SIM or 14 mg/kg DMXAA, drugs were injected intravenously on days 11 and 14 after tumor cell inoculation. Each experimental group consisted of 5 animals and the control group was treated with LCL (i.e. devoid of drug). At the end of the experiment (day 15) mice were euthanized using an euthanasia chamber and compressed CO_2 gas contained in a cylinder (Linde gaz, Romania). Animal experiments were performed according to the EU Directive 2010/63/EU and to the national regulations. The study is reported in accordance with ARRIVE guidelines and were approved by the Babes-Bolyai University Ethics Committee (Cluj-Napoca, Romania; Project ID: PN-II-RU-TE-2014–4–1191, Contract No. 235/01.10.2015, Approval no. 4335/19.03.2018).

Effects of different treatments on tumor growth. The effects of liposome-encapsulated agents SIM and DMXAA on tumor growth were compared to the effects of free active agents on B16.F10 murine melanoma-bearing mice. LCL-SIM (5 mg/kg) and LCL-DMXAA (14 mg/kg) were administered as monotherapies or combined, in the caudal vein of C57BL/6 mice, on days 11 and 14 after tumor cell inoculation. Mice from all experimental groups were sacrificed on day 15 and tumors were collected and stored in liquid nitrogen until analysis.

RT-qPCR determination of Arg-1 and iNOS mRNA expression. Total RNA was isolated from frozen tumors using an RNA kit (peqGOLD Total RNA Kit, PeqLab, Erlangen, DE). To avoid potential DNA contamination, 2 µg of total RNA were digested with 2U of RNase free DNase (Thermo Scientific, MA, USA) for 30 min at 37 °C, followed by addition of EDTA and incubation at 65 °C for 10 min. From the resulting DNA-free RNA, 1 µg was reverse-transcribed into cDNA using Verso cDNA kit (ThermoScientific, MA, USA), while identical samples from each experimental group processed in the absence of reverse transcriptase served as DNA contamination controls, as previously described[9]. Reverse transcription products (1 µl) were added to a 25 µl reaction mix containing 1 × Maxima SYBR Green qPCR Master Mix (Thermo Scientific, MA, USA) and 0.3 µM of each primer. Real-time PCR reactions were performed under the following cycling parameters: pre-incubation at 95 °C for 10 min, cycling: 95 °C for 15 s, 60 °C for 30 s, and then 72 °C for 30 s. Melting curves were generated to check for primer specificity. The primers used for gene amplification are presented in Table 1. Comparative Ct method (ΔΔCt) was used to calculate gene expression by relative quantitation. Gene expression was reported as fold change ($2^{-\Delta\Delta Ct}$), relative to mRNA expression in Control tumors, used as calibrator. Mouse β-actin mRNA was used as reference gene expression.

Name of genes	Forward primer (5′–3′)	Reverse primer(5′–3′)
Mouse *β-actin*	TCT TTG CAG CTC CTT CGT TGC CGG TCC	GTC CTT CTG ACC CAT TCC CAC CAT CAC AC
Mouse *ARG-1*	CTC CAA GCC AAA GTC CTT AGA G	AGG AGC TGT CAT TAG GGA CAT C
Mouse *iNOS*	TTC ACC CAG TTG TGC ATC GAC CTA	TCC ATG GTC ACC TCC AAC ACA AGA

Table 1. Forward and reverse primers used for RT-qPCR.

Angiogenic/inflammatory protein array analysis. To determine the effect of single and co-administered liposomal therapies on the expression levels of angiogenic/inflammatory proteins in whole tumor lysates, a screening for proteins involved in these major protumoral processes was performed, using the RayBio® Mouse Angiogenic protein Antibody Array membranes 1.1 (RayBiotech Inc., Norcross, GA, USA) as previously detailed[9,13]. Tumors from 5 mice/experimental group were pooled and lysed with Cell Lysis Buffer provided by manufacturer (1 ml lysis buffer per 1 mg tumor). Protease and phosphatase Inhibitor Cocktails (Sigma) were added to the lysis buffer. After the pooled tumor tissue lysates were obtained for each group, the protein content of the lysates was determined using Gornall method[15]. Further on, one array membrane was used per experimental condition and incubated with 250 µg protein from each lysate for 2 h, at room temperature. Each membrane contains 24 types of primary antibodies (in duplicate) against certain angiogenic proteins. In order to detect the level of expression of angiogenic/inflammatory proteins in tissue lysates we followed the manufacturer-provided protocol.

Histology and immunohistochemistry analysis. For the evaluation of histological features, the tumors were processed as previously described[14]. For immunohistochemistry, after paraffin embedding of tumors, 5 µm sections were cut and mounted on positively charged glass slides. The following primary antibodies were used: rabbit IgG anti-mouse CD31 (ab124432, Abcam, Cambridge, UK) diluted 1000-fold, rat IgG against mouse F4/80-diluted 250-fold (MCA497, Bio-Rad) and mouse IgG against mouse iNOS diluted 500-fold (sc-7271, Santa Cruz Biotechnology INC). The slides were examined by light microscopy and the positive reaction (area of the brown staining) was evaluated in at least ten different microscope fields. We used the following scoring system to evaluate the area percentage (%) of CD-31, F4/80 and iNOS positive immunoreaction: 0.5—5–20%; 1—20–40%; 2—40–60%; 3—60–80%; 4—80–100%.

Determination of nitric oxide metabolites in tumor lysates. To compare the effects of different liposomal treatments on the production of nitric oxide (NO), a key nitrosative stress marker produced by M1 macrophages via iNOS, we determined the levels of nitrite, the stable waste product of NO metabolism (Alupei et al. 2015). Tumor lysates were deproteinized with 5% sulfosalicilic acid (1:1, v/v). By adding Griess reagent to each sample, a pink-purple azo dye was formed in the presence of nitrite. The concentration of nitrite in each sample was determined based on the absorbance at 548 nm in relation to nitrite standards of known concentration. Data were expressed as nmoles of nitrite/g protein. Each sample was determined in triplicate.

Western Blot quantification of tumor tissue proteins. Frozen tumors from each experimental group were pooled to obtain tumor tissue lysates[16]. 5–10 µg proteins from each lysate were separated by SDS-PAGE onto a 10% polyacrylamide gel and immunobloted against the following primary antibodies, diluted 500-fold: mouse monoclonal IgG anti-mouse Bcl-xL (sc-8392, Santa Cruz Biotechnology, Texas, USA), rabbit polyclonal IgG anti-mouse Bax (2772S, Cell Signaling Technology, Inc, Danvers, USA), rabbit monoclonal IgG anti-mouse HIF-1α (ab179483, Abcam, Cambridge, UK), and rabbit polyclonal IgG anti-mouse pAP1-c-Jun (sc-7981-R, Santa Cruz Biotechnology, Texas, USA). β-actin which was used as loading control was detected using a rabbit polyclonal IgG against mouse β-actin (A2103, Merck, Darmstadt, GER) diluted 1000-fold. The nitrocellulose membranes were cut one band above and below the bands of the molecular weight marker that delimitates the protein of interest, prior to incubation with antibodies. For detection of the bound antibodies, goat anti-rabbit IgG HRP-labeled (sc-2004, Santa Cruz Biotechnology, Texas, USA) and goat anti-mouse IgG HRP-labeled antibodies (sc-2005, Santa Cruz Biotechnology, Texas, USA) diluted 4000-fold, were used. The immunocomplexes (formed by each protein and specific antibodies) were detected using chemiluminescence and X-ray films as previously reported[9]. Images of X-ray films were obtained by scanning the films, after exposing them to the NC membranes and to developer/fixer solutions. The X-ray films are stored in our laboratory, and the original images of the X-ray films are provided in Supplementary file.

Evaluation of oxidative stress parameters. The levels of lipid peroxidation marker MDA were measured by HPLC[17]. Data were normalized to the protein concentration in tumor lysates and expressed as nmoles MDA/mg protein. Intratumor activity of catalase was assessed using the method described by Aebi[18] and expressed as units of catalytic activity/mg protein. The evaluation of total antioxidant capacity (TAC) of the TME was performed according to the method described by Erel[19] and expressed as µmoles Trolox/mg protein. For these assays, each sample was determined in duplicate.

Gelatin zymography analysis of MMP-2 and MMP-9 activity. Electrophoretic gels containing 0.1% gelatin and 7.5% acrylamide were used to fractionate 30 µg proteins from tumor lysates, under denaturating but

LCLs	Size (nm)	PDI	Zeta potential (mV)	Therapeutic agent concentration (mg/ml)	Encapsulation efficiency (%)
LCL-SIM	135 ± 2.6	0.089	− 30	1.233	82.05
LCL-DMXAA	113 ± 3.8	0.079	− 41	2.367	39.7

Table 2. Characterization of LCL formulations encapsulating SIM or DMXAA.

non-reducing conditions. Determination of the gelatinolytic activity of MMP-2 and MMP-9 in tumor lysates followed previously published protocols[20].

Statistical analysis. Data from different experiments were expressed as mean ± standard deviation (SD). All statistical analyses were performed by using GraphPad Prism 9.2.0.332 (Serial number: GPS-2216002-E###-#####, MachineID: 3383874FBDD) (https://www.graphpad.com/). The overall effects of different treatments on tumor growth, on intratumor levels of anti-apoptotic proteins, key invasion and metastasis promoters and oxidative/nitrosative stress markers were analyzed by one-way ANOVA with Bonferroni correction for multiple comparisons. For the estimation of the treatments actions on angiogenic and inflammatory protein production, 2-way ANOVA with Bonferroni correction for multiple comparisons was used. The scores for immunoreaction intensities of tumor sections from different experimental groups were analyzed by using rank-based nonparametric Kruskall-Wallis test with Dunn's test for multiple comparisons. A P value of < 0.05 was considered significant.

Results

Characterization of liposomal drug formulations. As shown in Table 2, LCL-SIM and the novel LCL-DMXAA formulation were characterized regarding particle size distribution, polydispersity index, zeta potential, the concentration of the active drug and encapsulation efficiency. Importantly, mean particle size of the liposomes was found to be around 110–135 nm (below the cutoff limits of the pores of tumor endothelia which are 200–800 nm)[21], with a narrow size distribution (polydispersity index lower than 0.1, Table 2). Thus, given this attributes the liposomal formulation with SIM and DMXAA might have the ability to substantially extravasate and accumulate in tumors due to the enhanced permeability of tumor vasculature (referred to as the EPR "enhanced permeability and retention" effect), as compared to healthy endothelium[7,12,22]. Notably, the encapsulation efficiency values were very high for a hydrophobic drug such as SIM (over 80% for LCL-SIM) and for a hydrophilic drug such as DMXAA (about 40% for LCL-DMXAA), suggesting potential for future technological transfer of both liposomal formulations.

The combined liposomal drug therapy inhibited more effectively the growth of B16.F10 melanoma tumors than each single liposomal drug therapy. Antitumor efficiency of free and liposome-encapsulated drugs was evaluated by measuring daily the tumor volumes and analyzing the growth dynamics by the use of tumor growth curves (Fig. 1A,C,E), the tumor volume at day of sacrification (Fig. 1B,D,F), and the area under the tumor growth curve (AUTC) (Supplementary Figure 1 A, B, C). The volume of the tumors treated with LCL-SIM + LCL-DMXAA varied slightly from 140 mm^3 (at day 11) to 196 mm^3 (at day 15), compared to the volume of control tumors which increased almost 9-fold (from 195 mm^3 to 1700 mm^3 at day 15) while tumors treated with LCL-SIM or LCL-DMXAA had an average increase of 3.5–4 fold (Fig. 1A,C,E). Specifically, LCL-SIM administered alone strongly reduced (by 75–80%, $P < 0.05$, Fig. 1A,B and Supplementary Figure 1A) melanoma growth compared with administration of free SIM that was totally inefficient in terms of inhibition of tumor growth ($P > 0.05$, Fig. 1A,B and Supplementary Figure 1A). This was probably due to the tumor targeting properties of LCL. However, in the case of DMXAA, the encapsulation in LCL did not enhance the antitumor efficacy of the anti-angiogenic drug, since free DMXAA as well as the LCL form exerted similar antitumor activities on tumor growth (60–70% inhibition compared with control, $P < 0.05$, Fig. 1C,D, and Supplementary Figure 1B). Notably, both combined therapies (free or liposomal) suppressed melanoma growth strongly albeit with much higher degree, by 90–92% inhibition ($P < 0.001$) in the case of LCL-SIM + LCL-DMXAA drug therapy and by 60–65% inhibition ($P < 0.01$) after administration of free SIM in combination with DMXAA, compared with control (Fig. 1E,F and Supplementary Figure 1C). The effectiveness of the combined liposomal drug therapy against melanoma, demonstrated by almost total inhibition of tumor growth (starting with day 11, Fig. 1E) might be linked to the tumor targeting properties of the LCL as well as synergistic effect of the combined administration of SIM and DMXAA on melanoma cell proliferation, previously demonstrated by our group[9]. Therefore, given the strong antitumor effects of the combined liposomal therapy, the underlying molecular mechanisms of this novel therapeutic approach were further investigated by comparing the effects of single and combined LCL drug administration.

LCL-SIM co-administred with LCL-DMXAA partially "re-educated" TAMs by downregulating the mRNA expression of key arginine metabolic enzymes, iNOS and ARG-1. To investigate whether the suppressive effects exerted by combined liposomal therapy on the main TAMs-mediated pro-tumor processes can be associated with the capacity of this therapy to repolarize TAMs towards M1 phenotype, tumors were evaluated for the expression of iNOS and ARG-1 mRNA by RT-qPCR. iNOS and ARG-1 are specific markers for TAMs, a high Arg-1 activity defining the protumor M2 macrophages, while increased iNOS activity is

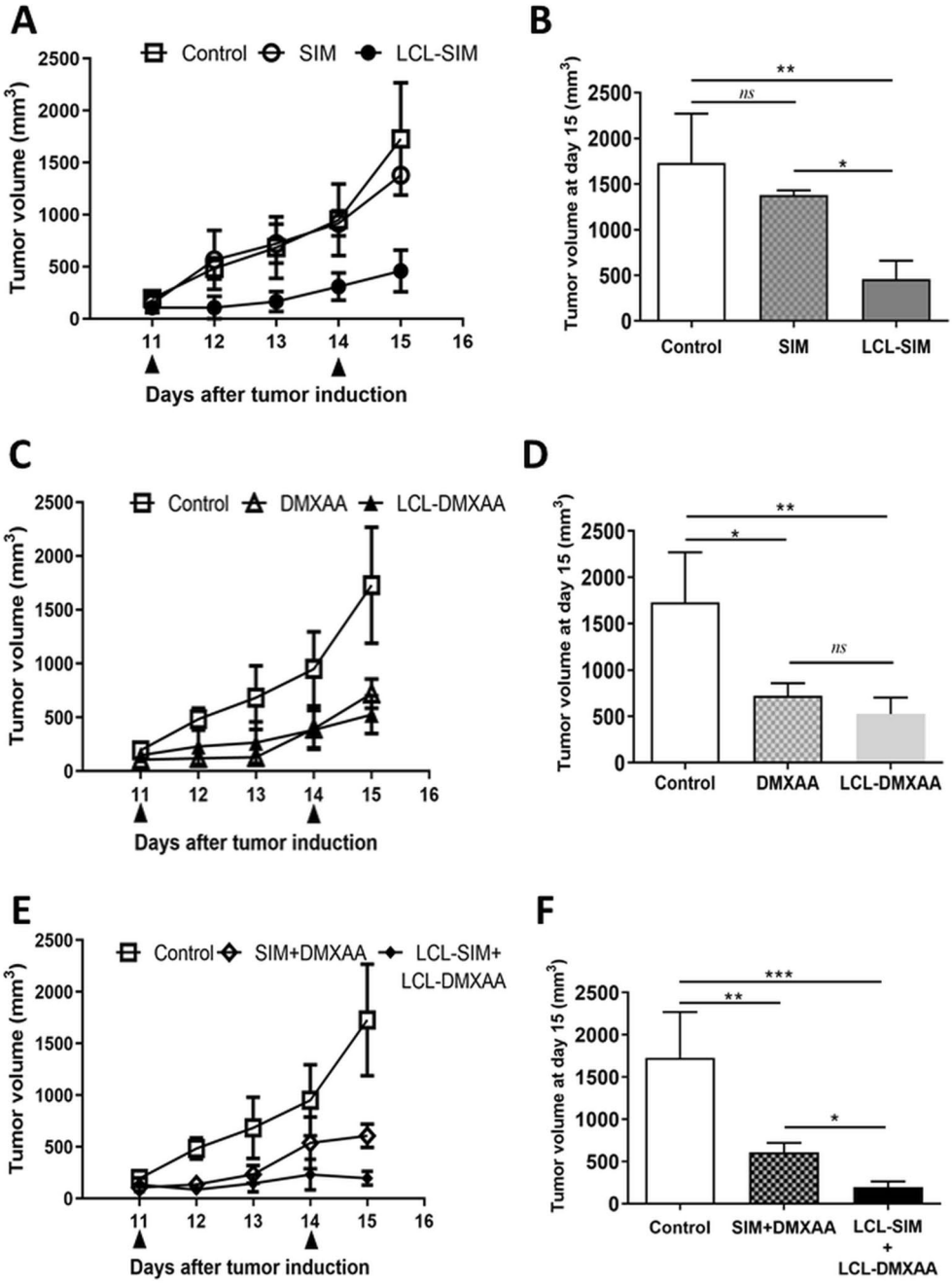

Figure 1. Effects of the combined administration of free and liposome-encapsulated SIM and DMXAA on the growth of *s.c.* B16.F10 murine melanoma. Mice received two *i.v.* injections of therapeutic agents at day 11 and day 14, after cancer cell inoculation. Tumor growth curves were presented in panels (**A**), (**C**), and (**E**). Tumor volumes after different treatments at day 15 (when mice were killed) were presented in panels (**B**), (**D**), and (**F**). Control—LCL-treated group; SIM—experimental group treated with 5 mg/kg free SIM; LCL-SIM—experimental group treated with 5 mg/kg SIM as liposome-encapsulated form; DMXAA—experimental group treated with 14 mg/kg free DMXAA; LCL-DMXAA—experimental group treated with 14 mg/kg DMXAA as liposome-encapsulated form; SIM + DMXAA—experimental group treated with 5 mg/kg free SIM and 14 mg/kg free DMXAA; LCL-SIM + LCL-DMXAA—experimental group treated with 5 mg/kg SIM and 14 mg/kg DMXAA as liposome-encapsulated forms. Results were expressed as mean ± SD of tumor volumes of 5 mice. One way ANOVA test with Bonferroni correction for multiple comparisons was performed to analyze the differences between the effects of the treatments on tumor growth (*ns*, $P > 0.05$; *, $P < 0.05$; **, $P < 0.01$; ***, $P < 0.001$). The graphs were generated using GraphPad Prism 9.2.0.332 (Serial number: GPS-2216002-E###-#####, MachineID: 3383874FBDD) (https://www.graphpad.com/).

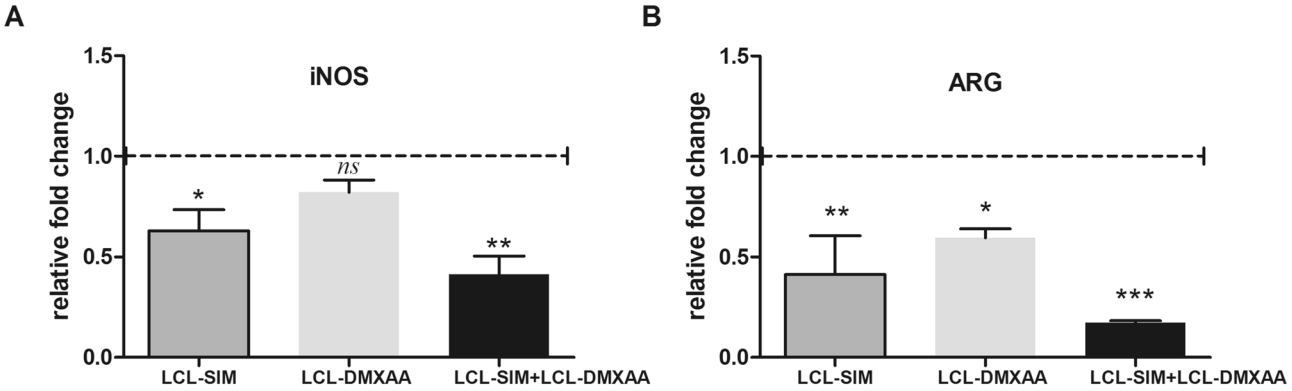

Figure 2. Effects of LCL-SIM and LCL-DMXAA single and combined treatment on the mRNA expression levels of enzymes involved in arginine metabolism in TME. (**A**), (**B**) Effects of liposomal SIM and DMXAA administration on the expression levels of iNOS and ARG-1. mRNA was quantified by RT-qPCR and the results were expressed as fold change based on the Ct calculations. Control—LCL-treated group was used as calibrator. Results were expressed as mean ± SD of three independent measurements. Control—LCL-treated group; LCL-SIM—experimental group treated with 5 mg/kg SIM as liposome-encapsulated form; LCL-DMXAA—experimental group treated with 14 mg/kg DMXAA as liposome-encapsulated form; LCL-SIM + LCL-DMXAA—experimental group treated with 5 mg/kg SIM and 14 mg/kg DMXAA as liposome-encapsulated forms. (*ns*, $P > 0.05$; *, $P < 0.05$; **, $P < 0.01$; ***, $P < 0.001$). The graphs were generated using GraphPad Prism 9.2.0.332 (Serial number: GPS-2216002-E####-#####, MachineID: 3383874FBDD) (https://www.graphpad.com/).

well-recognized as a key biomarker for antitumor M1 macrophages[23]. Our data indicated that LCL-SIM + LCL-DMXAA therapy induced the strongest reduction of mRNA expression levels for iNOS (Fig. 2A, $P < 0.01$, 0.41 relative fold change) and ARG-1 (Fig. 2B, $P < 0.001$, 0.17 relative fold change) compared to their mRNA expression level in Control group.

Combined treatment with LCL-SIM and LCL-DMXAA exerted strong anti-angiogenic effects on B16.F10 murine melanoma in vivo. To determine whether the antitumor activity of the combined liposomal drug therapy can be linked to its action on tumor angiogenesis, a screening for intratumor levels of 24 angiogenic/ inflammatory proteins was performed by protein microarray. In addition, the tumors were analyzed by immunohistochemistry with regard to the expression of CD31, a marker for proliferating endothelial cells[24] and of F4/80, a marker expressed on all murine macrophages.These cells play a pivotal role in the regulation of angiogenesis and tumor progression[25]. Since we already noticed treatment-induced changes in the expression of iNOS at the mRNA level, we also investigated the intratumor protein expression level of iNOS and production of nitrite, the stable and nonvolatile product of NO metabolism.

Our results showed (Fig. 3A and Table 3) that the production of almost all angiogenic/inflammatory proteins were inhibited to varying degrees by LCL-SIM (from 9% up to 70%) and by LCL-DMXAA (1–79%) monotherapies compared to control group. Combined liposomal treatment with SIM and DMXAA exerted the highest suppression (from 30% up to 95%) of the levels of key players involved in tumor angiogenesis and inflammation compared to their control levels. Specifically, compared to their control levels, potent pro-angiogenic/pro-inflammatory proteins such as MCP-1, IL-1α, IL-1β, IL-12p40, TNF-α, Leptin, Fas-L, b-FGF, G-CSF, M-CSF, IL-9, IL-13, GM-CSF were moderately to strongly reduced (by 48–72%), while the levels of IGF-II, a determinant of angiogenic sprouting[26] were reduced by 76% ($P < 0.01$) by the combined liposomal therapy. The levels of IL-6, which promotes defective angiogenesis in tumors[27] was reduced by 82% ($P < 0.001$) and the levels of eotaxin, a cancer cell invasion promoter[28] were reduced by 79% ($P < 0.01$). Notably, VEGF production suffered the most drastic suppression in the combination therapy treated experimental group (> 95%, $P < 0.001$), in correlation with the strong inhibition of HIF-1α (Fig. 6A,B). The average reduction of the proteins by LCL-SIM + LCL-DMXAA treatment was 20% higher compared to LCL-SIM treated group (Table 3 and Fig. 3A). Nevertheless, all anti-angiogenic proteins (TIMP-1, TIMP-2, PF-4, IL-12p70, IFN-γ, MIG) were moderately to strongly inhibited (by 30–76%) after the combined liposomal treatment with LCL-SIM + LCL-DMXAA.

Moreover, a significant reduction of CD31 expression in tumors that received treatments based on liposomal drugs (Fig. 3B, $P < 0.05$, and Supplementary Figure 2) was noticed, while the density of macrophages expressing F4/80 was not significantly altered by any of the liposomal therapies (Fig. 3C and Supplementary Figure 2) compared to control treatment. These findings might suggest a tight connection between inhibition of neovascularization and strong reduction of the production of pro-angiogenic proteins, confirming the strong anti-angiogenic properties of both SIM and DMXAA, already reported by us, in vitro[9]. Despite the treatment-induced changes in the expression of iNOS mRNA (Fig. 2A), its protein expression level (Fig. 3D and Supplementary Figure 2) and the production of nitrite were not significantly altered (Supplementary Figure 3, $P > 0.05$) by any of the liposomal drugs.

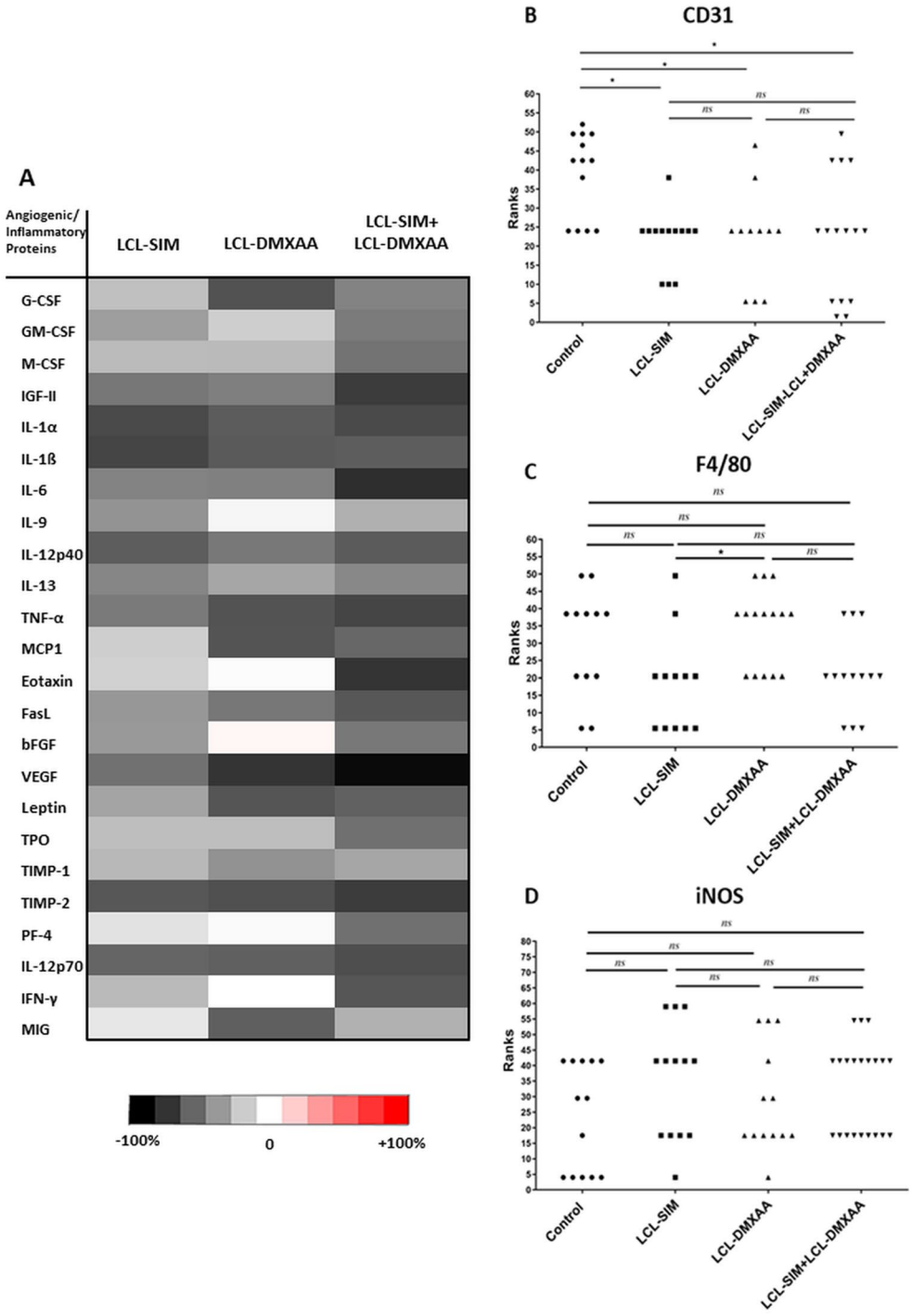

Figure 3. Effects of different treatments on angiogenic and inflammatory protein production and neovascularization in the tumor microenvironment. (**A**) Protein levels after different treatments were compared with the levels of the same proteins in control—LCL-treated group. Data are expressed as average % of reduction (–) of protein levels ranging from 0% (white) to − 100% (black) or stimulation (+) of production of proteins ranging from 0% (white) to + 100% (red) compared with the levels of the same proteins in control group. Immunohistochemical scores of (**B**) angiogenesis antigen CD31, (**C**) pan macrophage marker F4/80 and (**D**) M1 macrophage marker iNOS, in B16.F10 murine melanoma sections treated with free or liposomal SIM or/and DMXAA. The scores for immunoreaction intensities, obtained from minimum 10 random fields/condition, were analyzed by using rank-based nonparametric Kruskall-Wallis test with Dunn's test for multiple comparisons (*ns*, $P > 0.05$; *, $P < 0.05$). Control—LCL-treated group; LCL-SIM—experimental group treated with 5 mg/kg SIM as liposome-encapsulated form; LCL-DMXAA—experimental group treated with 14 mg/kg DMXAA as liposome-encapsulated form; LCL-SIM + LCL-DMXAA—experimental group treated with 5 mg/kg SIM and 14 mg/kg DMXAA as liposome-encapsulated forms. The graphs were generated using GraphPad Prism 9.2.0.332 (Serial number: GPS-2216002-E###-#####, MachineID: 3383874FBDD) (https://www.graphpad.com/). Multi-panel figure assembly and heatmap were generated using Microsoft® Office Home and Student 2019 MSO 64-bit (product ID: 00,405–57,743-39,916-AA493) (https://www.microsoft.com/).

Angiogenic/inflammatory proteins	Percentage of inhibition (–) and stimulation (+) of angiogenic/inflammatory protein production after different treatments compared to control group		
	LCL-SIM	LCL-DMXAA	LCL-SIM + LCL-DMXAA
G-CSF	– 24.48 ± 3.21 (*ns*)	– 67.54 ± 3.23 (*)	– 48.55 ± 2.46 (*)
GM-CSF	– 37.85 ± 2.88 (*ns*)	– 19.09 ± 4.97 (*ns*)	– 51.54 ± 2.76 (*)
M-CSF	– 26.45 ± 1.96 (*ns*)	– 26.69 ± 3.59 (*ns*)	– 54.67 ± 0.60 (*)
IGF-II	– 53.02 ± 0.21 (*)	– 50.08 ± 2.04 (*)	– 76.26 ± 1.02 (**)
IL-1α	– 70.92 ± 0.76 (**)	– 63.84 ± 1.49 (*)	– 70.61 ± 0.25 (**)
IL-1ß	– 72.57 ± 0.37 (*ns*)	– 64.40 ± 0.54 (*)	– 63.18 ± 1.76 (*)
IL-6	– 48.38 ± 4.26 (*)	– 49.77 ± 2.12 (*)	– 81.89 ± 0.95 (***)
IL-9	– 41.97 ± 2.97 (*)	– 3.31 ± 1.45 (*ns*)	– 30.88 ± 1.97 (*ns*)
IL-12p40	– 63.16 ± 3.06 (*)	– 52.78 ± 8.25 (*)	– 64.24 ± 0.13 (*)
IL-13	– 47.08 ± 0.66 (*)	– 34.86 ± 1.02 (*ns*)	– 46.36 ± 1.30 (*)
TNF-α	– 51.77 ± 4.01 (*)	– 67.40 ± 13.74 (*)	– 72.62 ± 0.62 (**)
MCP-1	– 19.02 ± 0.36 (*ns*)	– 66.68 ± 0.91(*)	– 59.22 ± 0.57 (*)
Eotaxin	– 17.98 ± 8.20 (*ns*)	– 1.08 ± 0.50 (*ns*)	– 79.38 ± 5.02 (**)
FasL	– 40.69 ± 1.31 (*)	– 53.07 ± 0.66 (*)	– 65.52 ± 0.63 (*)
bFGF	– 39.72 ± 1.81 (*ns*)	3.78 ± 0.82 (*ns*)	– 52.63 ± 0.48 (*)
VEGF	– 55.3 ± 3.72 (*)	– 79.24 ± 1.62(**)	– 95.83 ± 0.14 (***)
Leptin	– 35.57 ± 6.39 (*ns*)	– 66.56 ± 1.95 (*)	– 61.78 ± 6.35 (*)
Thrombopoietin	– 25.13 ± 0.27 (*ns*)	– 25.10 ± 5.84 (*ns*)	– 55.40 ± 3.41 (*)
TIMP-1	– 27.51 ± 2.37 (*ns*)	– 42.51 ± 4.58 (*)	– 34.59 ± 2.59 (*ns*)
TIMP-2	– 65.85 ± 2.06 (*)	– 68.50 ± 0.36 (*)	– 76.14 ± 0.91 (**)
PF-4	– 11.23 ± 3.04 (*ns*)	– 1.77 ± 2.65 (*ns*)	– 55.75 ± 0.42 (*)
IL-12p70	– 60.16 ± 2.15 (*)	– 62.32 ± 2.4 (*)	– 69.02 ± 1.4 (*)
IFN-γ	– 26.82 ± 5.73 (*ns*)	0.35 ± 0.66 (*ns*)	– 65.91 ± 1.33 (*)
MIG	– 9.04 ± 2.13 (*ns*)	– 62.72 ± 2.60 (*)	– 30.56 ± 28.50 (*ns*)

Table 3. The effects of LCL-SIM and LCL-DMXAA administered as single as well as combined treatment on TME angiogenic/inflammatory protein production. The angiogenic/inflammatory protein levels in tumor lysates after different treatments are compared to control– LCL-treated group levels of the same proteins. The results are expressed as % of the average inhibition (–) or stimulation (+) ± SD of two independent measurements. The two-way ANOVA Multiple Comparison Test was used to compare overall effects on the production of pro- /antitumor proteins in tumor lysates from all experimental groups ; LCL-SIM—experimental group treated with 5 mg/kg SIM as liposome-encapsulated form; LCL-DMXAA—experimental group treated with 14 mg/kg DMXAA as liposome-encapsulated form; LCL-SIM + LCL-DMXAA—experimental group treated with 5 mg/kg SIM and 14 mg/kg DMXAA as liposome-encapsulated forms (*ns*, $P > 0.05$; *, $P < 0.05$; **, $P < 0.01$; ***, $P < 0.001$).

Codelivery of liposomal SIM and DMXAA triggers apotosis in B16.F10 melanoma TME. To establish whether different treatments with liposomal SIM and DMXAA induced apoptosis in cells of melanoma TME, we assessed the relative expression levels of pro-apoptotic Bax and anti-apoptotic Bcl-xL proteins, by western blot. Our results revealed that only the combined treatment with liposomal SIM and DMXAA was able to upregulate Bax protein levels (Fig. 4A,B, $P < 0.05$), while all liposomal treatments down-regulated the intratumor production of the anti-apoptotic protein Bcl-xL compared to its level in control group (Fig. 4C,D, $P < 0.01$, $P < 0.05$). Overexpression of Bcl-xL is associated with chemoresistance and metastasis in melanoma and previous studies demonstrated that this protein competes with Bax, negatively influencing the mitochondrial membrane permeabilization[29,30]. Thus, the Bax/Bcl-xL protein expression ratio was determined and used as a good indicator to estimate the sensitivity of melanoma cells to applied drugs[31]. Our data showed that only LCL-SIM and LCL-SIM + LCL-DMXAA-treated tumors showed a 1.5-fold increase in Bax/Bcl-xL production ratio (Fig. 4E, $P < 0.05$) indicating that liposomal SIM sensitized melanoma cells to LCL-DMXAA therapy. The histopathological evaluation also revealed some morphological features of apoptosis induced by all liposomal treatments (Supplementary Figure 4A-D).

Effects of liposome-encapsulated SIM and DMXAA on intratumor oxidative stress. To link the anti-angiogenic properties of the liposomal therapies with any potential changes in intratumor oxidative stress, the levels of malondialdehyde (MDA), a product of lipid peroxidation, the activity of catalase and TAC were determined in tumor tissue lysates (Fig. 5). Our results suggested that both single liposomal therapies induced a weak increase in MDA levels (Fig. 5A, $P < 0.05$) whereas the combination liposomal therapy with SIM and DMXAA did not affect MDA levels (Fig. 5A, $P > 0.05$). In addition, a proportional decrease in enzymatic antioxidants (catalase) was noticed in tumor lysates from groups treated with LCL-SIM ($P < 0.05$), LCL-DMXAA

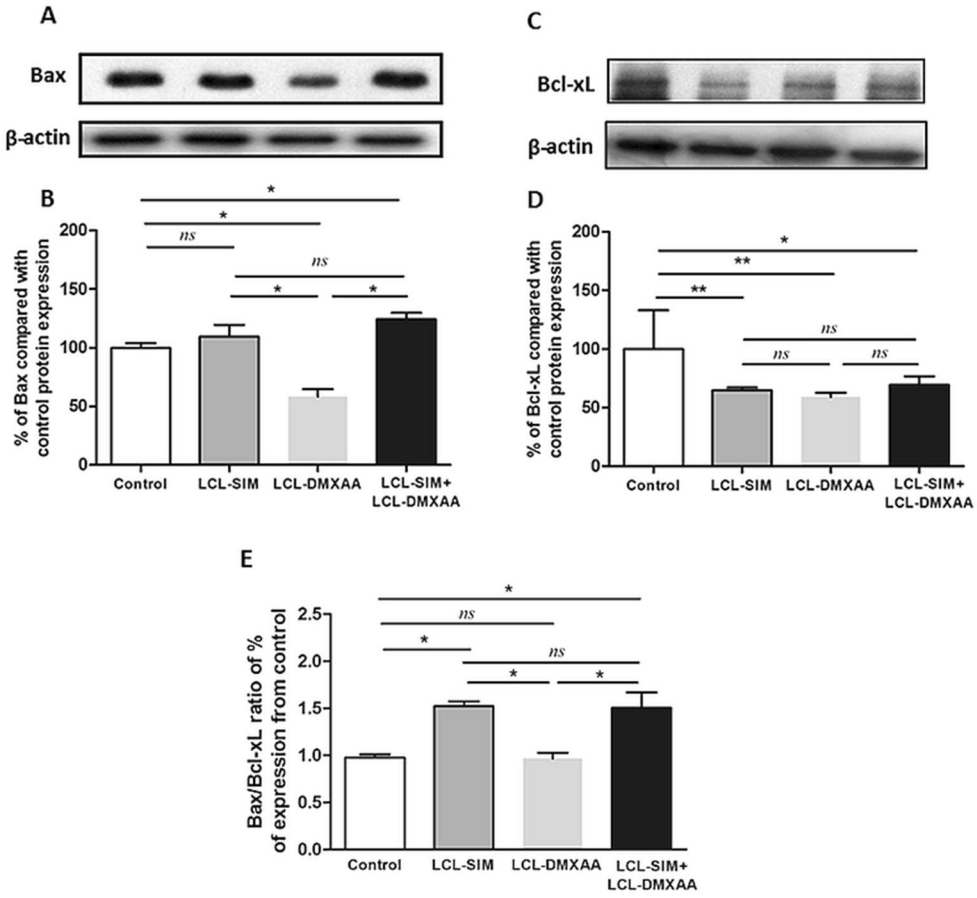

Figure 4. Effects of liposome-encapsulated SIM and DMXAA on intratumoral levels of apoptotic proteins. (**A**), (**B**) Western blot analysis showing the effects of different treatments on the intratumor levels of Bax and Bcl-xL, respectively. β-actin was used as loading control. (**C**), (**D**) Protein levels of Bax and Bcl-xL in lysates from treated groups expressed as percentage from control—LCL-treated group. (**E**) The ratio of % expression levels of Bax/Bcl-xL compared to Control. Data represent the mean ± SD of two independent measurements. One way ANOVA test with Bonferroni correction for multiple comparisons was performed to analyze the differences between the effects of the treatments on the apoptotic proteins (*ns*, $P > 0.05$; *, $P < 0.05$; **, $P < 0.01$). Control—LCL-treated group; LCL-SIM—experimental group treated with 5 mg/kg SIM as liposome-encapsulated form; LCL-DMXAA—experimental group treated with 14 mg/kg DMXAA as liposome-encapsulated form; LCL-SIM + LCL-DMXAA—experimental group treated with 5 mg/kg SIM and 14 mg/kg DMXAA as liposome-encapsulated forms. The uncropped images of Bax, Bcl-xL and β-actin blots are presented in Supplementary Information file. The graphs were generated using GraphPad Prism 9.2.0.332 (Serial number: GPS-2216002-E###-#####, MachineID: 3383874FBDD) (https://www.graphpad.com/). Images were processed using open source IrfanView graphic viewer 64-bit Version 4.58 (https://www.irfanview.com/) and multi-panel figure assembly was generated using Microsoft® Office Home and Student 2019 MSO 64-bit (product ID: 00405-57743-39916-AA493) (https://www.microsoft.com/).

($P < 0.01$) and the liposomal combination therapy (Fig. 5B, $P < 0.05$). Moreover, except for LCL-SIM treatment which did not affect the TAC ($P > 0.05$), all other treatments with LCL-DMXAA and LCL-DIM + LCL-DMXAA, significantly decreased TAC compared to control (Fig. 5C, $P < 0.01$ and $P < 0.05$ respectively).

Inhibitory effects of the combined liposomal drug therapy with SIM and DMXAA on melanoma invasion and metastasis promoters. The extent of tumor invasiveness and metastasis, after anti-angiogenic therapies depends on the coordinated interaction of numerous proteins and enzymes controlled by several transcription factors such as HIF-1α and AP-1[32–34]. Thus, we evaluated the impact of the combined liposomal therapy with SIM and DMXAA on intratumor production of metastatic promoters such as HIF-1α and pAP-1 c-Jun, and on the activity of MMP-2 and MMP-9, both of which are activated under hypoxia and degrade the extracellular matrix, facilitating cancer cell dissemination. In line with our previous studies[9], HIF-1α was strongly suppressed by the combined liposomal treatment (80% reduction compared to the protein production in control group) (Fig. 6A,B, $P < 0.001$), as opposed to single liposomal treatments which only elicited weak inhibitory effects (Fig. 6A,B, $P < 0.05$). Moreover, among all treatments tested, only the combined administration of LCL-SIM and LCL-DMXAA exerted an inhibitory effect on the production of pAP-1 c-Jun (by 47% compared

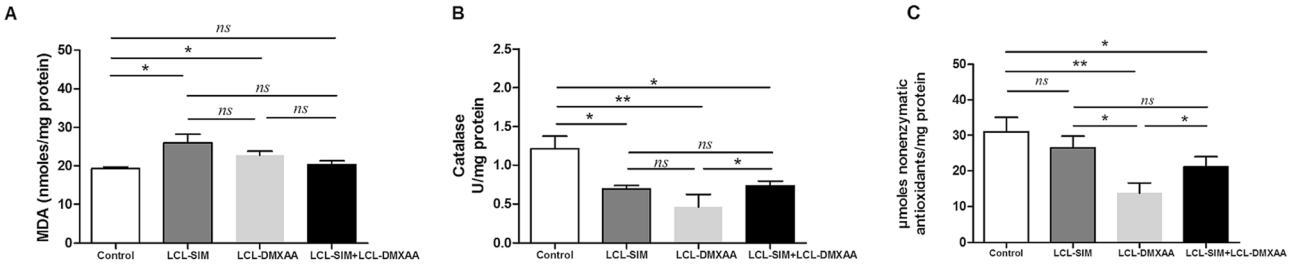

Figure 5. Effects of different liposomal treatments with SIM and DMXAA on tumor oxidative stress parameters. (**A**) MDA concentration expressed as nmoles MDA/mg protein; (**B**) Catalase activity expressed as U/mg protein; (**C**) TAC expressed as µmoles Trolox/mg protein. All parameters were measured in tumor lysates from mice treated with LCL-SIM and LCL-DMXAA as single or combined therapy. Data represent the mean ± SD of duplicate measurements (*ns*, $P > 0.05$; *, $P < 0.05$; **, $P < 0.01$). Control—LCL-treated group; LCL-SIM—experimental group treated with 5 mg/kg SIM as liposome-encapsulated form; LCL-DMXAA—experimental group treated with 14 mg/kg DMXAA as liposome-encapsulated form; LCL-SIM + LCL-DMXAA—experimental group treated with 5 mg/kg SIM and 14 mg/kg DMXAA as liposome-encapsulated forms. The graphs were generated using GraphPad Prism 9.2.0.332 (Serial number: GPS-2216002-E###-#####, MachineID: 3383874FBDD) (https://www.graphpad.com/).

to its control production, Fig. 6C,D). Activation of AP-1 is critically linked with Ras-induced oncogenic transformation in melanoma cells and tightly regulates the expression levels of both HIF-1α and MMPs metastatic promoters[33,35]. According to Fig. 6E–G, only the combined treatment notably decreased the lytic activity of both MMP-2 (80% inhibition compared to control, $P < 0.01$) and MMP-9 (70% inhibition compared to control, $P < 0.05$). Together, these results suggest that the reduction of intratumor production of HIF-1α and of pAP-1 c-Jun by combined liposomal therapy with LCL-SIM + LCL-DOX significantly weakened the invasive and metastatic ability of B16.F10 melanoma cells, via strong inhibition of MMPs activity.

Discussion

In the present study, we provide a follow-up of our earlier observations that liposomal SIM inhibited melanoma growth via concomitant suppressive actions on HIF-1α production in cancer cells and TAMs-mediated oxidative stress[7]. Moreover, these beneficial effects of SIM were recently exploited for the improvement of the anti-angiogenic action of DMXAA on B16.F10 melanoma cells cocultured with TAMs, when these drugs were co-administered[9]. Notably, these data have demonstrated synergistic antitumor action of SIM and DMXAA on an in vitro melanoma model via suppression of the aggressive phenotype of melanoma cells and TAMs re-education in TME. In the light of these earlier findings, we took the advantage of tumor targeting capacity of LCL to efficiently deliver SIM and DMXAA to B16.F10 melanoma in vivo with the final aim of improving the outcome of the anti-angiogenic therapy, which, to our knowledge, has never been described before.

Our study revealed that the administration of LCL-SIM + LCL-DMXAA therapy decelerated almost totally the growth of B16.F10 tumors in vivo, being superior as antitumor efficacy to each LCL-SIM or LCL-DMXAA therapy (Fig. 1A–F and Supplementary Figure 1). We believe that this effect was enabled by the tumor-targeting property of the LCL[22], and might be associated with the ability of LCL-SIM to partially "re-educate" TAMs[7,9] via modulation of arginine metabolism and inhibition of TAMs-driven angiogenesis[9]. As shown in Fig. 2B, mRNA expression data supports our previously published findings[9] regarding the beneficial association between SIM and DMXAA that successfully "re-educated" TAMs towards a M1 phenotype, by reducing ARG-1 expression. Thus, the abolishment of ARG-1 expression in TAMs was accompanied by subsequent deceleration of the M2 response and inhibition of polyamine synthesis, required for tumor cell proliferation, angiogenesis, cell invasion and metastasis[36]. This inhibitory effect might also mediate the enhancement of cytokine-dependent tumoricidal effects of T cells[37] in tumors. Although our combined liposomal therapy with SIM and DMXAA inhibited iNOS expression at mRNA level (Fig. 2A), certain regulatory mechanisms acting either posttranscriptionally or at translational level[38], maintained the production of intratumor iNOS, as reflected by its protein expression level (Fig. 3D and Supplementary Figure 2) and nitrite production (Supplementary Figure 3). In solid tumors, including melanoma, the fine regulation of ROS and NO concentration determines the development of cancer cells, and TAMs are important producers of sublethal levels of ROS and iNOS-derived NO[39]. Maintaining the production of this enzyme and of nitrite within the tumor physiological range, might be a beneficial effect of the combined liposomal therapy with SIM and DMXAA, by avoiding ROS-induced settlement of tumor cell resistance and hindering melanoma aggressiveness. Our data is supported by previous studies that linked the increase in ROS levels, after different therapies with inhibitors of the BRAF and MEK kinases, with ROS-induced resistance to treatments, in melanoma cells or in animal/patient tumors[40,41]. Accordingly, our results showed that LCL-SIM + LCL-DMXAA therapy failed to enhance the level of physiological oxidative stress in the tumors (Fig. 5A).

This beneficial action of the combined liposomal therapy on TAMs re-education towards an antitumor phenotype was tightly connected to the enhancement of the anti-angiogenic effects of LCL-DMXAA, by LCL-SIM co-administration (Fig. 3A, Table 3). In our previous studies we have shown that the antitumor activity of LCL-SIM is dependent on tumor oxidative stress suppression[7]. However, our present data suggested that the antitumor efficacy of LCL-SIM administered as monotherapy or in combination with LCL-DMXAA, is highly dependent on tumor angiogenesis suppression (Fig. 3A, B, Table 3 and Supplementary Figure 2). Although they did not affect

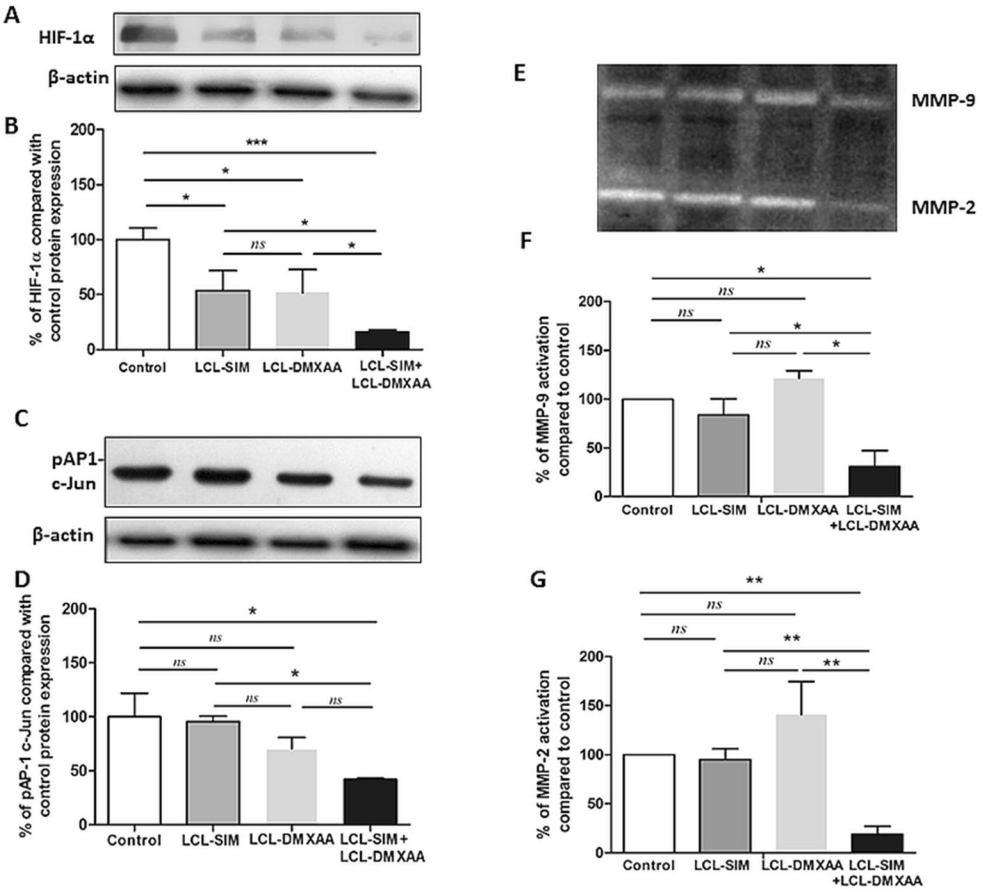

Figure 6. Effects of liposome-encapsulated SIM and DMXAA on intratumoral levels of key invasion and metastasis promoters. (**A**), (**C**) Western blot analysis showing the effects of different treatments on the intratumor levels of HIF-1α and pAP-1 c-Jun, respectively. β-actin was used as loading control. (**B**), (**D**) Protein levels of HIF-1α and pAP-1 c-Jun in lysates from treated groups expressed as percentage from Control—LCL-treated group. Data represent the mean ± SD of two independent measurements. One way ANOVA test with Bonferroni correction for multiple comparisons was performed to analyze the differences between the effects of the treatments on apoptotic proteins (*ns*, $P > 0.05$; *, $P < 0.05$; ***, $P < 0.001$). (**E**), (**F**), (**G**)—The effects of different treatments on the activity of microenvironmental matrix metalloproteinases. (**E**) Gelatin zymography analysis of tumor lysates from mice treated with various liposome-encapsulated SIM and DMXAA therapies. Coomassie blue staining highlights gelatinolytic activity corresponding to MMP-9 and MMP-2 (pro-froms and active forms). (**F**), (**G**) Percentage of MMP-9 and MMP-2 activity in tumor lysates from mice treated with single and combined SIM and DMXAA liposomal therapies compared to control. Data represent the mean ± SD of two independent measurements. One way ANOVA test with Dunnett correction was performed to analyze the differences between the effects of various treatments on MMP-9 and MMP-2 levels compared to control untreated group (*ns*, $P > 0.05$; *, $P < 0.05$; **, $P < 0.01$). Control—LCL-treated group; LCL-SIM—experimental group treated with 5 mg/kg SIM as liposome-encapsulated form; LCL-DMXAA—experimental group treated with 14 mg/kg DMXAA as liposome-encapsulated form; LCL-SIM + LCL-DMXAA—experimental group treated with 5 mg/kg SIM and 14 mg/kg DMXAA as liposome-encapsulated forms. The uncropped images of HIF-1α, pAP-1 c-Jun and β-actin blots, as well as the uncropped gel showing MMP-9 and MMP-2 gelatinolytic activity are presented in Supplementary Information file. The graphs were generated using GraphPad Prism 9.2.0.332 (Serial number: GPS-2216002-E###-#####, MachineID: 3383874FBDD) (https://www.graphpad.com/). Images were processed using open source IrfanView graphic viewer 64-bit Version 4.58 (https://www.irfanview.com/) and multi-panel figure assembly was generated using Microsoft® Office Home and Student 2019 MSO 64-bit (product ID: 00405-57743-39916-AA493) (https://www.microsoft.com/).

the number of macrophages, key drivers of tumor angiogenesis, (Fig. 3C and Supplementary Figure 2), both LCL-SIM and LCL-SIM-DMXAA therapies strongly suppressed the most powerful pro-angiogenic protein VEGF (with more than 55% and 95% respectively, compared to its control level, Fig. 3A and Table 3) and significantly reduced the density of blood vessels compared to their density in control tumor tissue (Fig. 3B, $P < 0.05$). It is known that altered expression of VEGF has been found to correlate with melanoma stage and progression[42] and that its targeting appears to offer some therapeutic benefit in melanoma patients, when combined with chemo- or immunotherapy[43]. Altogether, these data imply that the antitumor actions of LCL-SIM, when co-administered

with LCL-DMXAA, depends on the predominant protumor process driving tumor growth in relation to the stage and the volume of the tumor. In line with our findings, several studies confirm these variable and apparently disparate effects of various anticancer treatments[44,45].

The major drawback of current anti-angiogenic therapies is represented by the hypoxia-induced drug resistance in cancer cells, supported by activation of HIF-1 pathways[46]. As a consequence, a compensatory upregulation of alternative pro-angiogenic molecules occurs in the TME, allowing cancer cells to resist apoptosis and to acquire a more invasive and metastatic behaviour[6]. Therefore, to gain further insight into the LCL-SIM-mediated sensitization of TME to the effects of LCL-DMXAA, we evaluated the impact of this combined therapy on important markers defining TME resistance profile and aggressiveness. Noteworthy, the combined therapy with LCL-SIM and LCL-DMXAA strongly reduced (by 50–81%) the intratumor production of bFGF, IL-1 α/β, IL-6, TNFα, leptin and of eotaxin, which allow cancer cells to escape VEGF-targeted therapies, promoting tumor growth and metastasis[47,48]. Moreover, it seemed that this combined liposomal therapy did not induce the settlement of cancer cell resistance to anti-angiogenic drugs, as treated tumors showed 1.5-fold increase of the Bax/Bcl-xL production ratio (Fig. 4E, $P < 0.05$) and presented several morphological hallmarks of apoptosis (Supplementary Figure 4D). Other studies also confirmed that anti-apoptotic proteins such as Bcl-2 and Bcl-xL are highly expressed in melanoma[49] and a high Bcl-2/Bax or Bcl-xL/Bax ratio correlates with the resilience of cancer cells to undergo apoptosis[31]. Thus, the enhanced intratumor production of pro-apoptotic Bax protein and the strong reduction of intratumor production of IL-6 and Fas-L (Figs. 3A, 4A, B and Table 3), which are of critical importance for cancer cell survival, demonstrate the sensitivity of tumor cells to the combined liposomal therapy and indicate induction of apoptosis[9,13,31,50].

Evidence of accentuated invasiveness of tumor cells following evasive resistance to anti-angiogenic therapy[51], determined us to further assess the effect of our treatments on several established promoters of tumor progression and metastasis (Fig. 6) such as MMPs. Therefore, the intratumor activity of both MMP-9 and MMP-2, that are involved in facilitating cancer cell dissemination at secondary sites, was investigated by zymography. Although SIM exerts suppressive effects on expression and activation of MMPs[52] and on melanoma cell migration capacity when co-administered with DMXAA[9], our data suggested no significant modulation of MMP-2 and MMP-9 lytic activity by either LCL-SIM or LCL-DMXAA (Fig. 6E–G, $P > 0.05$). Notably, when the liposomal drugs were administered concurrently, the activity of both MMP-9 (Fig. 6E–G, $P < 0.05$) and MMP-2 (Fig. 6E–G, $P < 0.01$) was reduced to a different extent (by 70% and 80%, respectively). An explanation for these findings might be given by the similar impact of this treatment on the intratumor production of critical pro-angiogenic/pro-invasive proteins (VEGF, bFGF, IL-1α, IL-1β, IL-6, TNF-α, and eotaxin, Fig. 3A, Table 3) and most importantly, on the production of transcription factors HIF-1α and pAP-1 c-Jun (Fig. 6A–D). Both HIF-1α and pAP-1 c-Jun proteins are key players in cancer cells resistance to anti-angiogenic therapies and activate distinct transcriptional programs that converge to coordinate ECM degradation and metastasis, via MMPs[33,53]. Thus, the combined liposomal therapy strongly suppressed the intratumor production of HIF-1α (by 84% $P < 0.001$) and of pAP-1 c-Jun (by 47%, $P < 0.05$) proteins compared to their control production (Fig. 6A–D). Altogether, in spite of the fact that several studies associated the therapeutic inhibition of angiogenesis with increased tumor cell invasiveness[54], our data suggested that by codelivering LCL-SIM together with LCL-DMXAA, the tumor beneficial association between the activation of HIF-1α/VEGF axis and MMP-2/9 activation[55,56] was blunted.

Conclusions

Taken together, our results showed that the combined liposomal therapy inhibited almost totally the growth of melanoma tumors, due to the enhancement of anti-angiogenic effects of LCL-DMXAA by LCL-SIM and induction of a pro-apoptotic state of tumor cells in the TME. These effects were accompanied by the partial "re-education" of TAMs towards an M1 antitumor phenotype and augmented by combined treatment-induced suppression of major invasion and metastasis promoters (HIF-1α, pAP-1 c-Jun, and MMPs).

Data availability

The data sets generated during and/or analysed during the current study are available from the corresponding author on reasonable request.

Received: 21 June 2021; Accepted: 26 October 2021
Published online: 11 November 2021

References

1. Mahabeleshwar, G. H. & Byzova, T. V. Angiogenesis in melanoma. *Semin. Oncol.* **34**, 555–565 (2007).
2. De Palma, M., Biziato, D. & Petrova, T. V. Microenvironmental regulation of tumour angiogenesis. *Nat. Rev. Cancer* **17**, 457–474 (2017).
3. Ellis, L. M. & Hicklin, D. J. VEGF-targeted therapy: mechanisms of anti-tumour activity. *Nat. Rev. Cancer* **8**, 579–591 (2008).
4. Liang, W., Ni, Y. & Chen, F. Tumor resistance to vascular disrupting agents: mechanisms, imaging, and solutions. *Oncotarget* **7**, 15444–15459 (2016).
5. Tazzyman, S., Murdoch, C., Yeomans, J., Harrison, J. & Muthana, M. Macrophage-mediated response to hypoxia in disease. *Hypoxia (Auckl)* **2**, 185–196 (2014).
6. Haibe, Y. *et al.* Resistance mechanisms to anti-angiogenic therapies in cancer. *Front. Oncol.* **10**, 221 (2020).
7. Alupei, M. C., Licarete, E., Patras, L. & Banciu, M. Liposomal simvastatin inhibits tumor growth via targeting tumor-associated macrophages-mediated oxidative stress. *Cancer Lett.* **356**, 946–952 (2015).
8. Cassetta, L. & Pollard, J. W. Targeting macrophages: therapeutic approaches in cancer. *Nat. Rev. Drug Discov.* **17**, 887–904 (2018).
9. Rauca, V.-F. *et al.* Combination therapy of simvastatin and 5, 6-dimethylxanthenone-4-acetic acid synergistically suppresses the aggressiveness of B16.F10 melanoma cells. *PLoS ONE* **13**, e0202827 (2018).

10. Tang, K. *et al.* Hypoxia-reprogrammed tricarboxylic acid cycle promotes the growth of human breast tumorigenic cells. *Oncogene* **38**, 6970–6984 (2019).
11. Dominiak, A., Chełstowska, B., Olejarz, W. & Nowicka, G. Communication in the cancer microenvironment as a target for therapeutic interventions. *Cancers (Basel)* **12**, E1232 (2020).
12. Banciu, M., Fens, M. H. A. M., Storm, G. & Schiffelers, R. M. Antitumor activity and tumor localization of liposomal glucocorticoids in B16 melanoma-bearing mice. *J. Control Release* **127**, 131–136 (2008).
13. Banciu, M., Schiffelers, R. M., Fens, M. H. A. M., Metselaar, J. M. & Storm, G. Anti-angiogenic effects of liposomal prednisolone phosphate on B16 melanoma in mice. *J. Control Release* **113**, 1–8 (2006).
14. Licarete, E. *et al.* Overcoming intrinsic doxorubicin resistance in melanoma by anti-angiogenic and anti-metastatic effects of liposomal prednisolone phosphate on tumor microenvironment. *Int. J. Mol. Sci.* **21**, 2968 (2020).
15. Gornall, A. G., Bardawill, C. J. & David, M. M. Determination of serum proteins by means of the biuret reaction. *J. Biol. Chem.* **177**, 751–766 (1949).
16. Luput, L. *et al.* In vivo double targeting of C26 colon carcinoma cells and microenvironmental protumor processes using liposomal simvastatin. *J. Cancer* **9**, 440–449 (2018).
17. Licarete, E. *et al.* HIF-1α acts as a molecular target for simvastatin cytotoxicity in B16.F10 melanoma cells cultured under chemically induced hypoxia. *Oncol. Lett.* **13**, 3942–3950 (2017).
18. Aebi, H. Catalase in vitro. *Methods Enzymol.* **105**, 121–126 (1984).
19. Erel, O. A novel automated direct measurement method for total antioxidant capacity using a new generation, more stable ABTS radical cation. *Clin. Biochem.* **37**, 277–285 (2004).
20. Sesarman, A. *et al.* Co-delivery of curcumin and doxorubicin in PEGylated liposomes favored the antineoplastic C26 murine colon carcinoma microenvironment. *Drug Deliv. Transl. Res.* **9**, 260–272 (2019).
21. Porfire, A. *et al.* Optimizing long-circulating liposomes for delivery of simvastatin to C26 colon carcinoma cells. *J. Liposome Res.* **25**, 261–269 (2015).
22. Schiffelers, R. M. *et al.* Liposome-encapsulated prednisolone phosphate inhibits growth of established tumors in mice. *Neoplasia* **7**, 118–127 (2005).
23. Sica, A. & Mantovani, A. Macrophage plasticity and polarization: in vivo veritas. *J. Clin. Invest.* **122**, 787–795 (2012).
24. Miettinen, M., Lindenmayer, A. E. & Chaubal, A. Endothelial cell markers CD31, CD34, and BNH9 antibody to H- and Y-antigens–evaluation of their specificity and sensitivity in the diagnosis of vascular tumors and comparison with von Willebrand factor. *Mod. Pathol.* **7**, 82–90 (1994).
25. Banciu, M., Metselaar, J. M., Schiffelers, R. M. & Storm, G. Antitumor activity of liposomal prednisolone phosphate depends on the presence of functional tumor-associated macrophages in tumor tissue. *Neoplasia* **10**, 108–117 (2008).
26. Dallinga, M. G. *et al.* IGF2 and IGF1R identified as novel tip cell genes in primary microvascular endothelial cell monolayers. *Angiogenesis* **21**, 823–836 (2018).
27. Gopinathan, G. *et al.* Interleukin-6 stimulates defective angiogenesis. *Cancer Res.* **75**, 3098–3107 (2015).
28. Zhu, F., Liu, P., Li, J. & Zhang, Y. Eotaxin-1 promotes prostate cancer cell invasion via activation of the CCR3-ERK pathway and upregulation of MMP-3 expression. *Oncol Rep.* **31**, 2049–2054 (2014).
29. Billen, L. P., Kokoski, C. L., Lovell, J. F., Leber, B. & Andrews, D. W. Bcl-XL inhibits membrane permeabilization by competing with Bax. *PLoS Biol.* **6**, e147 (2008).
30. Choi, S. *et al.* Bcl-xL promotes metastasis independent of its anti-apoptotic activity. *Nat. Commun.* **7**, 10384 (2016).
31. Raisova, M. *et al.* The Bax/Bcl-2 ratio determines the susceptibility of human melanoma cells to CD95/Fas-mediated apoptosis. *J Invest. Dermatol.* **117**, 333–340 (2001).
32. Rankin, E. B. & Giaccia, A. J. Hypoxic control of metastasis. *Science* **352**, 175–180 (2016).
33. Bergman, M. R. *et al.* A functional activating protein 1 (AP-1) site regulates matrix metalloproteinase 2 (MMP-2) transcription by cardiac cells through interactions with JunB-Fra1 and JunB-FosB heterodimers. *Biochem. J.* **369**, 485–496 (2003).
34. Dratkiewicz, E. *et al.* Hypoxia and extracellular acidification as drivers of melanoma progression and drug resistance. *Cells* **10**, 862 (2021).
35. Kappelmann, M., Bosserhoff, A. & Kuphal, S. AP-1/c-Jun transcription factors: regulation and function in malignant melanoma. *Eur. J. Cell Biol.* **93**, 76–81 (2014).
36. Soda, K. The mechanisms by which polyamines accelerate tumor spread. *J. Exp. Clin. Cancer Res.* **30**, 95 (2011).
37. Ley, K. M1 Means Kill; M2 means heal. *J. Immunol.* **199**, 2191–2193 (2017).
38. Aktan, F. iNOS-mediated nitric oxide production and its regulation. *Life Sci.* **75**, 639–653 (2004).
39. Monteiro, H. P. *et al.* Nitric oxide and interactions with reactive oxygen species in the development of melanoma, breast, and colon cancer: A redox signaling perspective. *Nitric Oxide* **89**, 1–13 (2019).
40. Wang, L. *et al.* An acquired vulnerability of drug-resistant melanoma with therapeutic potential. *Cell* **173**, 1413-1425.e14 (2018).
41. Yuan, L. *et al.* BRAF mutant melanoma adjusts to BRAF/MEK inhibitors via dependence on increased antioxidant SOD2 and increased reactive oxygen species levels. *Cancers (Basel)* **12**, E1661 (2020).
42. Mabeta, P. Paradigms of vascularization in melanoma: clinical significance and potential for therapeutic targeting. *Biomed. Pharmacother.* **127**, 110135 (2020).
43. Jour, G., Ivan, D. & Aung, P. P. Angiogenesis in melanoma: an update with a focus on current targeted therapies. *J. Clin. Pathol.* **69**, 472–483 (2016).
44. Zhu, X.-Y. *et al.* Disparate effects of simvastatin on angiogenesis during hypoxia and inflammation. *Life Sci.* **83**, 801–809 (2008).
45. Siemann, D. W. & Rojiani, A. M. The vascular disrupting agent ZD6126 shows increased antitumor efficacy and enhanced radiation response in large, advanced tumors. *Int. J. Radiat. Oncol. Biol. Phys.* **62**, 846–853 (2005).
46. Masoud, G. N. & Li, W. HIF-1α pathway: role, regulation and intervention for cancer therapy. *Acta Pharm. Sin. B* **5**, 378–389 (2015).
47. Itatani, Y., Kawada, K., Yamamoto, T. & Sakai, Y. Resistance to anti-angiogenic therapy in cancer-alterations to anti-VEGF pathway. *Int. J. Mol. Sci.* **19**, 1232 (2018).
48. Fisher, D. T., Appenheimer, M. M. & Evans, S. S. The two faces of IL-6 in the tumor microenvironment. *Semin. Immunol.* **26**, 38–47 (2014).
49. Lee, E. F. *et al.* BCL-XL and MCL-1 are the key BCL-2 family proteins in melanoma cell survival. *Cell Death Dis.* **10**, 342 (2019).
50. Berthenet, K. *et al.* Failed apoptosis enhances melanoma cancer cell aggressiveness. *Cell Rep.* **31**, 107731 (2020).
51. Bergers, G. & Hanahan, D. Modes of resistance to anti-angiogenic therapy. *Nat. Rev. Cancer* **8**, 592–603 (2008).
52. Tsubaki, M. *et al.* Statins improve survival by inhibiting spontaneous metastasis and tumor growth in a mouse melanoma model. *Am. J. Cancer Res.* **5**, 3186–3197 (2015).
53. Hanna, S. C. *et al.* HIF1α and HIF2α independently activate SRC to promote melanoma metastases. *J. Clin. Invest.* **123**, 2078–2093 (2013).
54. Lugano, R., Ramachandran, M. & Dimberg, A. Tumor angiogenesis: causes, consequences, challenges and opportunities. *Cell Mol. Life Sci.* **77**, 1745–1770 (2020).
55. Sun, B. *et al.* Hypoxia influences vasculogenic mimicry channel formation and tumor invasion-related protein expression in melanoma. *Cancer Lett.* **249**, 188–197 (2007).
56. Lv, X. *et al.* The role of hypoxia-inducible factors in tumor angiogenesis and cell metabolism. *Genes Dis.* **4**, 19–24 (2017).

Author contributions

Conceptualization and study design: V.F.R., M.B.; Funding acquisition: M.B., V.F.R., A.S.; Execution: V.F.R., L.P., L.L., E.L., V.A.T., A.P., A.C.M., A.S.: Acquisition of data: V.F.R., L.P., L.L., E.L., V.A.T., A.P., A.C.M., A.S.; Analysis and interpretation: V.F.R., A.S., M.B.; Writing—original draft: V.F.R., A.S.; Review & editing: A.S., E.R.T., M.B.

Funding

This work was funded by UEFISCDI (Romanian Ministry of Research and Innovation), under Grant PN-II-RU-TE-2014–4–1191 (No. 235/01.10.2015), by Babeş-Bolyai University under Grants for Young Researchers (No. 35282/18.11.2020), Grants for the support of strategic infrastructure for 2020 (33PFE/2018 and CNFIS-FDI-2020–0387) and by Deutsche Forschungsgemeinschaft (DFG, German Research Foundation)—Project-ID 360372040—SFB 1335.

Competing interests

The authors declare no competing interests.

Additional information

Supplementary Information The online version contains supplementary material available at https://doi.org/10.1038/s41598-021-01284-5.

Correspondence and requests for materials should be addressed to A.S.

Reprints and permissions information is available at www.nature.com/reprints.

Publisher's note Springer Nature remains neutral with regard to jurisdictional claims in published maps and institutional affiliations.